Order Reconstruction Phenomena and Temperature-Driven Dynamics in a 3D Zenithally Bistable Device

A. Raisch[1] and A. Majumdar[2]

[1] *Oxford Centre for Collaborative Applied Mathematics, University of Oxford - OX1 3LB, United Kingdom*
[2] *Department of Mathematical Sciences, University of Bath - Bath, BA2 7AY, United Kingdom*

PACS 61.30.Jf – Disclinations of Liquid Crystals
PACS 02.30.Jr – Partial differential equations
PACS 42.79.Kr – Liquid Crystals in optical devices

Abstract – We model the Zenithally Bistable Device (ZBD) in three dimensions (3D), within the Landau-de Gennes theory, and find three stable static states in 3D without an applied field: the Vertically Aligned (VAN) state, the Hybrid Aligned (HAN) state and a third, high-tilt state, which we call the THAN state, with an interior and a surface defect. We recover the (OR) phenomenon around the defects in the HAN and THAN states and the 3D THAN and HAN solutions exhibit stable biaxial cylinders connecting defects on opposite faces of the ZBD device. We demonstrate two-way temperature-driven switching between high-tilt and low-tilt states through controlled heating and cooling procedures in two dimensions (2D), with no applied fields.

Introduction. – Nematic liquid crystals (LCs) are anisotropic liquids with long-range orientational ordering that have widespread applications in science and industry [1]. This combination of fluidity and preferred directions leads to unique electro-optic properties and notably, nematics form the backbone of the huge liquid crystal display (LCD) industry [2]. There is now significant interest in controlling nematic alignment using patterned surfaces in micro-confined or nano-confined geometries [3–6]. These confined systems exhibit a rich variety of spatio-temporal patterns, the modelling of which presents new mathematical and computational challenges and opens new doors for LC-based applications.

The ZBD is an example of a micropatterned LCD that has been very successful for retail applications [7]. There is an industrial company named, "ZBD Solutions", specializing in electronic shelf labels based on the ZBD device [8]. A typical ZBD geometry consists of a LC layer sandwiched between two surfaces, one of which is planar and the other is featured by a sinusoidal grating [7]. The sinusoidal or non-planar grating makes this relatively simple ZBD geometry experimentally "bistable", in the sense that there are at least two stable optically contrasting states: the Vertically Aligned Nematic (VAN) state and the Hybrid Aligned Nematic (HAN) state [7, 9]. The VAN state is a defect-free high-tilt state that is opaque to incident light whereas the transparent HAN state has a low-tilt profile around the sinusoidal grating with two defects close to the apex and to the trough of the grating, respectively. Both states exhibit long-term stability and contrasting optical properties, in the absence of electric fields, and applied fields are only required to switch between the different states, or equivalently to update an image. There are now several generalizations of the ZBD that include asymmetric gratings, periodic channels, two-sided ZBD, etc. [10].

The ZBD has received substantial interest in the modelling community, since the complex geometry and topological defects present new questions related to multistability, optimal grating structures and switching mechanisms [5, 9–11]. In this paper, we model a prototype ZBD in 3D (to be defined below) within the celebrated Landau-de Gennes (LdG) theory. In particular, we do not use any dimensional reduction and allow the structural details to depend on all three spatial coordinates. We work with temperatures below but close to the critical supercooling temperature and hence, our results are not "low-temperature" effects although we expect that they will hold deep in the nematic phase, too. We primarily focus on static studies, *i.e.*, the structure of stable equilibria in 2D and 3D. In both 2D and 3D, we find a third stable state, in addition to the known VAN and HAN states, labelled as the THAN state. The THAN state is a high-tilt state with a $+1/2$ defect pinned to the trough of the grating and an interior $-1/2$ defect vertically above it. The

THAN state is numerically stable (in the absence of electric fields) and persists for asymmetric sinusoidal gratings as will be explained below.

We numerically probe into the defects in the HAN and THAN state and find localized biaxial rings or order-reconstruction (OR) phenomena around them [12]. The phrase "OR phenomena" originates from the seminal paper [13] and has subsequently been used to describe static defect structures and dynamic defect-mediated phenomena in theoretical and experimental papers [3, 4, 12, 14]. OR phenomena typically describe defect structures with a uniaxial defect core that has negative order parameter, surrounded by a biaxial ring that connects to a far-field uniaxial state with positive order parameter; such defect structures have been found in both macroscopic and microscopic LC theories [12,14–16]. In light of previous work, one would expect to see the OR phenomenon around the defects in the HAN and THAN states and our 3D approach captures the OR phenomenon and the associated characteristics in the ZBD. We do not enforce translational invariance and yet, the biaxial rings around the defects do not shrink or disappear in the ZBD interior but exhibit translational invariance and extend as stable biaxial cylinders into the ZBD interior. The existence of translationally invariant solutions (such as the biaxial cylinders) is not surprising but the long-term stability of these solutions opens up the possibility of observable biaxiality on micron-scales, which is interesting from both a scientific and applications point of view. Our 3D results are complemented by a detailed 2D study of the relative stabilities of the VAN, HAN and THAN states as a function of temperature and geometrical parameters, along with grating asymmetry and elastic anisotropy. We present mutlistability squares to illustrate the interplay between temperature and co-existence/multistability. On the dynamics side, we report new two-way temperature-driven, field-independent switching mechanisms between high-tilt and low-tilt states in two dimensions and similar annealing processes in 3D. The transient dynamics are mediated by "biaxial" interfaces pinned to the sinusoidal grating and strongly resemble field-induced switching reported in [17]. At this stage, our results focus on biaxiality and temperature-dominated effects in a prototype 3D ZBD that are of intrinsic modelling interest and illustrate the rich solution landscape of the ZBD.

Modelling. – We model the ZBD device as a 3D cell,

$$\Omega = \left\{(x, y, z) \in \mathbb{R}^3; 0 \leq x, y \leq D; f(x) \leq z \leq H\right\}, \quad (1)$$

where $f(x) = \delta \sin 2\pi x + \delta$ denotes the bottom sinusoidal grating. The two geometrical parameters are the cell height, $H\mu m$, and the grating amplitude, $\delta\mu m$. We take $D = 1\mu m$ as a typical length scale for a micron-scale device. The front and rear surfaces are in the (x, z)-plane and the normal is in the y-direction. In fact, a lot of the previous work has focussed on 2D modelling in the (x, z)-plane alone [9, 11, 17] and the authors average over the normal direction. However, we do not have a "thin" geometry, the x and y-dimensions are comparable and hence, we allow all variables to depend on (x, y, z)-coordinates. In accordance with existing literature [9–11], we impose normal boundary conditions on the top and bottom surfaces: $z = f(x)$ and $z = H$; planar boundary conditions on the front and rear surfaces, $y = 0$ and $y = D$; and periodic conditions on the lateral surfaces, $x = 0$ and $x = D$. The planar boundary conditions require the LC molecules to be in the (x, z)-plane on $y = 0$ and $y = D$, and there is no single distinguished direction. The ZBD has been modelled in 3D at a fixed temperature, in [18] but with a different geometry that has slips between periodically repeated gratings. These slips serve to stabilize line defects and multiple states. We have the simplest 3D version of the ZBD, a translational extension in the normal direction. It serves as a good model system to explore biaxiality, temperature-dominated and geometry-dominated effects.

The LdG theory describes the state of a nematic LC by a macroscopic order parameter that quantifies the degree of orientational anisotropy: the $\mathbf{Q}$-tensor order parameter [1, 5]. The LdG $\mathbf{Q}$-tensor is a symmetric, traceless 3×3 matrix with three eigenvalues, $\{\lambda_i\}$, $i = 1 \ldots 3$ and $\sum_{i=1}^{3} \lambda_i = 0$. A LC is said to be in the isotropic phase if $\mathbf{Q} = 0$, uniaxial phase if $\lambda_i = \lambda_j \neq 0$ for some $i \neq j$, and biaxial phase if $\lambda_i \neq \lambda_j$ for any i, j [1, 19]. A uniaxial $\mathbf{Q}$-tensor can be concisely expressed as $\mathbf{Q} = s\left(\mathbf{n} \otimes \mathbf{n} - \mathbf{I}/3\right)$, where $\mathbf{n}$ is the distinguished eigenvector with the non-degenerate eigenvalue and s is a scalar order parameter that measures the degree of order about $\mathbf{n}$. A biaxial $\mathbf{Q}$-tensor necessarily has two distinguished directions/eigenvectors with two associated order parameters. The biaxiality parameter, $\beta^2(\mathbf{Q}) = 1 - 6\left(\left(\mathrm{tr}\mathbf{Q}^3\right)^2 / \left(\mathrm{tr}\mathbf{Q}^2\right)^3\right)$ is a measure of the degree of biaxiality; it takes values in the range $\beta^2 \in [0, 1]$ and $\beta^2(\mathbf{Q}) = 0$ iff $\mathbf{Q}$ is purely uniaxial [12, 14]. The stable equilibria correspond to local minimizers of an appropriately defined LdG energy functional (with no electric fields) [1, 5]:

$$I_{LdG}(\mathbf{Q}) = I_E(\mathbf{Q}) + I_B(\mathbf{Q}) + I_N(\mathbf{Q}) + I_T(\mathbf{Q}). \quad (2)$$

Here,

$$\begin{aligned}
I_E(\mathbf{Q}) &= \frac{L}{2}\int_\Omega |\nabla \mathbf{Q}|^2 \, dV \\
I_B(\mathbf{Q}) &= \int_\Omega \frac{A(T)}{2}\mathrm{tr}\mathbf{Q}^2 - \frac{B}{3}\mathrm{tr}\mathbf{Q}^3 + \frac{C}{4}\left(\mathrm{tr}\mathbf{Q}^2\right)^2 \, dV \\
I_N(\mathbf{Q}) &= \frac{W}{2}\int_{z_-=f(x), z_+=H} \left|\mathbf{Q} - \mathbf{Q}_{\nu_\pm^z}\right|^2 \, dA \\
I_T(\mathbf{Q}) &= \frac{W}{2}\int_{y_-=0, y_+=D} \left|\nu_\pm^y \mathbf{Q} \nu_\pm^y + \frac{s_0}{3}\right|^2 \, dA, \quad (3)
\end{aligned}$$

$\nu_\pm^z$ ($\nu_\pm^y$) denotes the normal to the surfaces, $z = H$ and $z = f(x)$ ($y = D$ and $y = 0$) respectively and,

$s_0(A) = (B + \sqrt{B^2 - 24AC})/4C$, is a constant. The first contribution, I_E, is the one-constant/isotropic elastic energy that penalizes spatial distortions and $L > 0$ is an elastic constant [5]. The fourth-order bulk energy, I_B, drives the first-order nematic-isotropic transition, $A(T) = \alpha(T - T^*)$, T^* is a critical supercooling temperature below which the isotropic phase loses stability and $\alpha, B, C > 0$ are material-dependent constants. One can explicitly show that the minimizers of I_B are either uniaxial or isotropic and the preferred degree of bulk order is $s_0(A)$, for temperatures $T < T^*$ [19]. Informally speaking, the bulk energy f_B coerces energy minimizers to be "uniaxial" almost everywhere and biaxiality is believed to be dominant near defects or interfaces. We work with weak anchoring and employ two different surface energies: (i) I_N, which is a Durand-Nobili type of anchoring energy that enforces uniaxial normal boundary conditions on $z = f(x)$ and $z = H$, with $\mathbf{Q}_\nu = s_0\,(\nu \otimes \nu - \mathbf{I}/3)$ [20] and (ii) I_T, which enforces uniaxial tangent boundary conditions on the surfaces, $y = 0$ and $y = D$, *i.e.*, the integrand $\nu_\pm^y \mathbf{Q} \nu_\pm^y + s_0/3$ vanishes if $\mathbf{Q}$ is uniaxial of the form, $\mathbf{Q} = s_0(A)\,(\mathbf{n} \otimes \mathbf{n} - \mathbf{I}/3)$ with $\mathbf{n} \cdot \nu_\pm^y = 0$ [5]. There are other forms of tangent surface energies but I_T suffices for our purposes.

We non-dimensionalize the LdG energy using the following scalings: $\tilde{\mathbf{Q}} = \mathbf{Q}/s_0$; $\tilde{I}_{LG} = I_{LG}/(LDs_0^2)$, $D\tilde{\Omega} = \Omega$. The re-scaled bulk and anchoring coefficients are given by $\tilde{A}(T) = (D^2\alpha(T - T^*))/L$, $\tilde{B} = (BD^2 s_0)/L$, $\tilde{C} = (CD^2 s_0^2)/L$ and $\tilde{W} = (WD)/L$. Typical values of the material-dependent constants are $L = 1.55 * 10^{-11}\,\mathrm{N}$, $\alpha = 0.042 * 10^6\,\mathrm{Nm^{-2}K^{-1}}$, $B = 6.4 * 10^5\,\mathrm{Nm^{-2}}$, $C = 3.5 * 10^5\,\mathrm{Nm^{-2}}$, $W \in \left(10^{-8}, 10^{-3}\right)\,\mathrm{Nm^{-1}}$ [5], so that the re-scaled anchoring coefficient, $\tilde{W} \in \left(10^{-3}, 10^2\right)$ [10].

Tristability in 3D. – We introduce two quantitative measures for distinguishing between different equilibria: (i) the biaxiality measure, $\Psi_1(\mathbf{Q}) = \max_{\mathbf{r}\in\Omega} \beta^2(\mathbf{Q})$ and (ii) the tilt measure, $\Psi_2(\mathbf{Q}) = (1/\delta)\int_{\Omega\cap\{2\delta\le z\le 3\delta\}} (\mathbf{n}_Q \cdot \hat{\mathbf{z}})^2\, dy$, where $\hat{\mathbf{z}}$ is the unit-vector in the z-direction and $\mathbf{n}_Q$ is the leading eigenvector of $\mathbf{Q}$ or equivalently the eigenvector with the largest positive eigenvalue. The first measure, Ψ_1, tracks regions of enhanced biaxiality. The tilt measure, Ψ_2, is a measure of the tilt above the grating and differentiates between high-tilt and low-tilt equilibria. We define an equilibrium to be in the (i) **VAN** state if $\Psi_1(\mathbf{Q}) \le 0.5$ and $\Psi_2(\mathbf{Q}) > 0.5$, (ii) **THAN** state if $\Psi_1(\mathbf{Q}) = 1$ and $\Psi_2(\mathbf{Q}) \ge 0.5$ and (iii) **HAN** state if $\Psi_1(\mathbf{Q}) = 1$ and $\Psi_2(\mathbf{Q}) < 0.5$. These threshold values are arbitrary and qualitative trends will be unchanged for different reasonable threshold values.

In fig. 1, we find three equilibria at temperature $T = (T^* - 1)$, labelled as VAN, HAN and THAN, according to the definitions above, all of which are numerically stable. Here, we use a variety of different initial conditions and these initial conditions relax into one of the three states mentioned above. The corresponding leading eigenvectors and biaxiality measures are plotted on the cross section

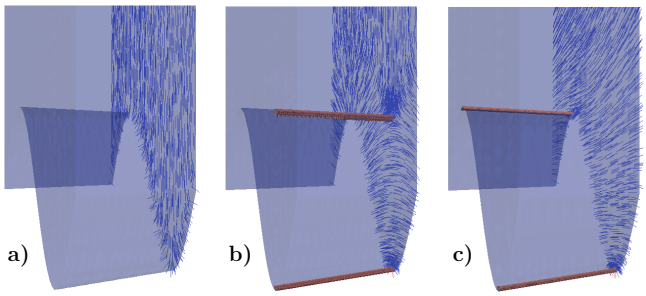

Fig. 1: Three stable states in the ZBD at temperature $T = (T^* - 1)$ Kelvin: (a) VAN state, (b) THAN state and (c) HAN state. We plot the leading eigenvector on the cross-section $y = 1$ along with biaxial domains with $\beta(Q) > 0.1$. While the VAN state is uniaxial in the whole of the cell, we observe cylinders of maximal biaxiality in the THAN state (stacked on top of each other) and HAN state (pinned to the apex and to the trough of the grating).

$y = 1$. The VAN state has a defect-free, high-tilt profile with negligible bulk biaxiality. There are two defects in the THAN state; a $+1/2$ defect pinned to the trough of the grating and a $-1/2$ defect vertically above it in the ZBD interior. The HAN state has a low tilt profile around the grating with two surface defects, the $-1/2$ defect is pinned to the apex and the $+1/2$ defect is pinned to the trough of the grating respectively. The THAN state has been previously observed as a transient state in field-induced dynamics in [6] but we find numerical evidence of its stability in the absence of an electric field. We have repeated these computations with asymmetric gratings of the form, $f(x) = \delta \sin(2\pi x + 0.3\sin(2\pi x))$, and an anisotropic elastic energy density $2w_e = L_1|\nabla\mathbf{Q}|^2 + L_2\mathbf{Q}_{ij,j}\mathbf{Q}_{ik,k}$, where $L_2/L_1 \approx 0.69$ [5]. The THAN state is found with both an asymmetric grating and elastic anisotropy.

In fig. 2, we study the eigenvalue profiles of the HAN state at different heights in the ZBD cell. Away from the grating, the HAN state is perfectly uniaxial (with very small β^2, within numerical resolution) with two coincident eigenvalues. We plot the biaxiality parameter across the defect core on the surface $y = 0$ and observe two peaks of maximal biaxiality on either side of the $-1/2$-degree defect. Then, we plot the eigenvalues across the apex defect core and observe (i) a bulk uniaxial state with positive order parameter outside the defect core, (ii) a biaxial ring that encloses the defect core, (iii) a core uniaxial state with negative order parameter of the form, $\mathbf{Q} = s\,(\mathbf{y} \otimes \mathbf{y} - \mathbf{I}/3)$ where $\mathbf{y}$ is the unit-vector in the y-direction and $s < 0$. In particular, the LC molecules are disordered in the (x, z)-plane, inside the defect core, on $y = 0$. This is characteristic of the OR or "eigenvalue exchange" phenomenon as two eigenvalues are swapped when we traverse a defect core [3, 4, 12]. In fig. 3, we plot $\beta^2(\mathbf{Q})$ throughout the 3D domain and find that (apart from boundary effects on $y = 0$ and $y = 1$) the biaxial rings are translationally

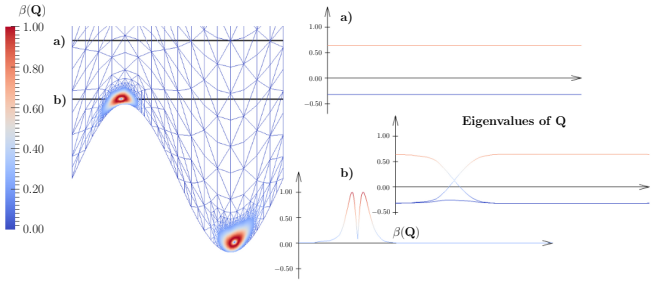

Fig. 2: HAN state: Biaxiality measure β on a slice of the cell (left), eigenvalues of $\mathbf{Q}$ at two different heights (right). At (a), the $\mathbf{Q}$-tensor is perfectly uniaxial with two degenerate eigenvalues and at (b) the $\mathbf{Q}$-tensor has three distinct eigenvalues around the defect core. The second plot at (b) is $\beta(\mathbf{Q})$ across the defect core with two peaks of maximal biaxiality.

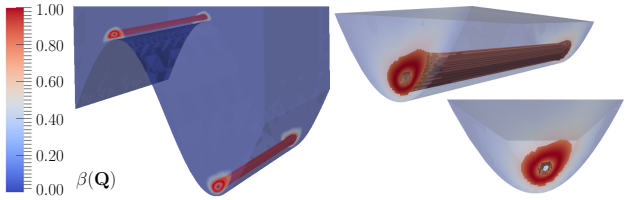

Fig. 3: Biaxial cylinder in the 3D HAN state: We plot the isosurface for $0.7 < \beta(\mathbf{Q}) < 1$ (left), and zoom into the trough of the grating (right). One can clearly observe an extension in the y-direction along with uniaxial defect cores.

invariant in the normal y-direction, i.e. they extend as a co-axial cylinder that connects two biaxial rings on the front and rear surfaces, $y = 0$ and $y = 1$, respectively, with macroscopic length along the entire device width. In other words, the HAN and THAN solutions constitute a class of translationally invariant equilibria for the ZBD cell, where a line defect extends along the device length. The leading eigenvector is oriented in the y-direction, along the defect lines. This is, of course, admissible but it is noteworthy that we do not find solutions that break the translational symmetry in the y-direction. For example, there may exist solutions where the leading eigenvector escapes into the (xz)-plane for $0 < y < 1$ or solutions where biaxiality is confined to a small neighbourhood of the defects on $y = 0$ and $y = 1$, for example see the single-core, double-core and split-core 3D solutions reported in [21]. Indeed, we may find such solutions as we move to lower temperatures, for which biaxiality is energetically expensive or for cells with the y-dimension much larger than the x-dimension. There is an energetic penalty associated with line defects and if line defects are very long (e.g. for a long ZBD), it might be energetically preferable to distort the line defect.

We report a temperature-driven switching mechanism between the VAN and HAN states, in 3D, as illustrated in fig. 4. The initial temperature is, $T_i = T^* - 0.25K$, with the VAN state as initial condition. The VAN state is almost uniaxial everywhere but there is a weakly biaxial boundary layer pinned to the grating surface. We heat the system to $T_f = T^* + 1K$ and cool it down to T_i again with a linear time-dependent temperature profile, see fig. 4, and model the dynamics with a L^2-gradient flow [22]. The L^2-gradient flow is based on the principle that the LdG energy is decreasing with time and the governing partial differential equation is

$$\gamma \frac{\partial \mathbf{Q}}{\partial t} = \nabla \cdot \left(\frac{\partial e\left(\mathbf{Q}, \nabla \mathbf{Q}\right)}{\partial \nabla \mathbf{Q}} \right) - \frac{\partial e\left(\mathbf{Q}, \nabla \mathbf{Q}\right)}{\partial \mathbf{Q}_{ij}} \tag{4}$$

where $\gamma > 0$ is a viscosity coefficient and $e\left(\mathbf{Q}, \nabla \mathbf{Q}\right)$ is the LdG energy density (see (2)). At time $t = 1$, we observe enhanced biaxiality along the grating and the system starts to relax towards a lower-tilt state. For longer times $t > 1$, the system settles into the stable HAN state as the biaxial interfacial layers shrink to the defects at the apex and trough of the grating respectively. There are no applied fields here but the switching proceeds through the creation of defects along the grating surface, analogous to field-induced switching reported in [17]. More realistic dynamical models (with electric fields) have been analyzed in [23, 24] and we refer the reader to [24] for a dynamical numerical model for the OR phenomenon.

2D modelling. – In the previous section, we perform computationally expensive simulations of a 3D $\mathbf{Q}$-tensor (with five degrees of freedom) that depends on (x, y, z)-spatial coordinates. An intermediate modelling approach is to simulate a 3D $\mathbf{Q}$-tensor that only depends on two spatial coordinates; see [15] where the authors use this approach to model square wells. In this section, we perform traditional simulations of a 2D $\mathbf{Q}$-tensor on a 2D domain, to further investigate the role of temperature in multistability. The non-dimensional 2D domain is

$$\Omega_D = \left\{(x, z) \in \mathbb{R}^2; 0 \leq x \leq 1 \text{ and } f(x) \leq z \leq H\right\}. \tag{5}$$

We impose normal boundary conditions on the curves, $z = f(x)$ and $z = H$, through a Durand-Nobili energy of the type, I_N, in (2) along with free boundary conditions on the edges, $x = 0$ and $x = 1$.

In 2D, the $\mathbf{Q}$-tensor is a symmetric, traceless 2×2 matrix, $\mathbf{Q} = s\left(\mathbf{n} \otimes \mathbf{n} - \mathbf{I}/2\right)$ [20]. Therefore, a 2D $\mathbf{Q}$-tensor has only two degrees of freedom (as opposed to five in 3D), $\mathrm{tr}\mathbf{Q}^3 = 0$ in 2D and the biaxiality parameter, $\beta^2(\mathbf{Q})$, has no physical meaning here. The defects are solely contained in the isotropic set, $\Gamma = \{(x, y) \in \Omega_D; s(x, y) = 0\}$ and we track the zero-set to study defects in 2D problems [20]. We use $\Psi_1(\mathbf{Q}) := \min_{r \in \Omega} |\mathbf{Q}|$ in the 2D definition of VAN, HAN and THAN states. The stable equilibria are local minimizers of a dimensionless LdG energy:

$$I_{LG}[\mathbf{Q}] := \frac{1}{2} \int_\Omega |\nabla \mathbf{Q}|^2 + \frac{1}{\epsilon^2} \left(|\mathbf{Q}|^2 - 1\right)^2 dA + I_N(\mathbf{Q}) \tag{6}$$

where I_N is the normal anchoring energy as in (2) and $\epsilon = (2\sqrt{L})/(D\sqrt{\alpha(T^* - T)})$ for $T < T^*$. We work with

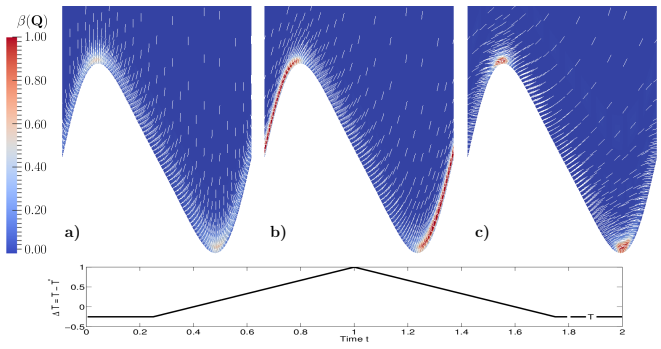

Fig. 4: Switching by temperature: (a) the initial VAN state, (b) the system switches to a HAN state at $t = 1$ and (c) stays in the HAN state after cooling down.

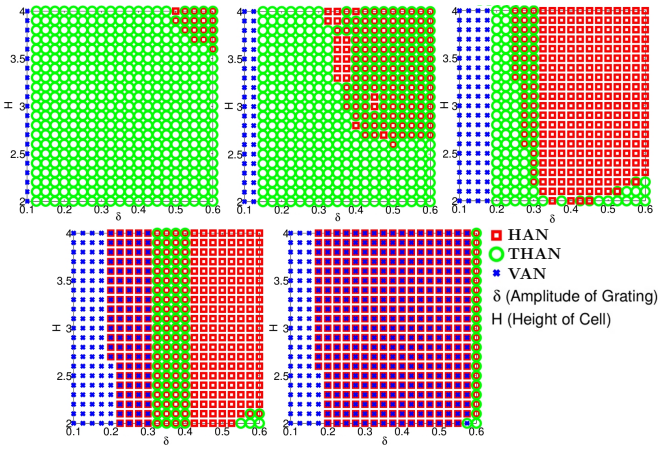

Fig. 5: Multistability squares: From left to right and top to bottom we present the computed multistability squares for $\epsilon = 2^{-i}$, $i = 1 \dots 5$, with $H \in (2, 4)$ and $\delta \in (0.1, 0.6)$. We use strong anchoring with fixed boundary conditions, $\mathbf{Q} = \mathbf{Q}_\nu$, on $z = f(x)$ and $z = H$. We observe a broader bistability regime for low temperatures, no HAN states for shallow gratings and no VAN states for deep gratings.

temperatures $T < T^*$ and for a given T, ϵ is proportional to the temperature-dependent nematic correlation length or equivalently, to a characteristic defect core size [1, 12].

We use finite element methods to numerically compute local energy minima (6), with five different values of $\epsilon = 2^{-i}, i = 1 \dots 5$ that correspond to temperatures $T^* - T \in \left(3 * 10^{-3}, 0.74\right)$, *i.e.*, temperatures close to the critical supercooling temperature. The numerical algorithm is a standard combination of L^2-gradient flow and Newton's iteration algorithm [22]. For every set of parameters (H, δ, ε), we run our algorithm twice, with two sets of initial data, mimicking the VAN and HAN profiles respectively. The outputs are recorded with a blue cross (VAN), a green circle (THAN) or a red square (HAN) in the multistability squares in fig. 5. These states co-exist over a range of (H, δ) and arise from a subtle competition between distortion energy around the grating and energy cost of defects.

We have repeated these 2D computations using a range of physically realistic values of $\tilde{W} \in (50, 200)$ [10], with asymmetric gratings of the form, $f(x) = \delta \sin(2\pi x + 0.3 \sin(2\pi x))$, and an anisotropic elastic energy density $2w_e = L_1 |\nabla \mathbf{Q}|^2 + L_2 \mathbf{Q}_{ij,j} \mathbf{Q}_{ik,k}$, where $L_2/L_1 \approx 0.69$ [5]. The reader is referred to [25] for stability studies with electric fields for a 2D ZBD and to [26] for stability studies on other 2D micropatterned surfaces.

In 2D, we can achieve two-way switching between high-tilt and low-tilt states through a controlled heating and cooling procedure. We take $(\delta, H) = (0.3, 3)$, with anchoring coefficient, $\tilde{W} = 40$. For $\epsilon_0 = 0.5$, the system is monostable with the THAN state being the unique stable state. For smaller values of ϵ, *e.g.* $\epsilon_1 = 0.05, 0.25$, the cell is bistable with two coexisting states: the HAN state and the THAN state, although the HAN state is energetically preferred. We first heat the system from ϵ_1 to ϵ_0 with a linear profile as in fig. 4 with the HAN state as initial condition in (i) and with the THAN state as initial condition in (ii). The resulting equilibrium, both for (i) and (ii), at time $t = 1$, is the THAN state as expected. In a quasi-static cooling procedure, we decrease the temperature from ϵ_0 to ϵ_1 with a linear profile and two different cooling rates, (i) $\chi_f = 10^{-3}$ and (ii) $\chi_{sl} = 6{*}10^{-6}$, respectively. For each updated value ϵ_{new}, we compute a new equilibrium, $\mathbf{Q}_{\epsilon_{new}}$ with the previous equilibrium, $\mathbf{Q}_{\epsilon_{old}}$, as initial condition, till we hit the final value, ϵ_1. The final state depends on the cooling rate, see fig. 6 (left). This can be explained as follows: (i) the THAN state is 'frozen' for fast cooling with $\chi_f = 10^{-3}$ and there is switching from HAN to THAN, see fig. 6 (right) and (ii) the system has more time to adapt to its environment for slower cooling with $\chi_{sl} = 6{*}10^{-6}$, enters the energetically preferred HAN branch and stays therein. Thus, we have achieved switching from THAN to HAN. The energy barriers have been computed and are high enough to ensure the robustness of this procedure. Using (i) and (ii) together, we can switch between high-tilt and low-tilt states.

We have modelled the ZBD in a 3D LdG framework and our modelling demonstrates field-independent biaxiality and temperature-dominated features in the ZBD. Firstly, we have found a third stable THAN state in 2D and 3D ZBD cells, even with asymmetric gratings. This shows that there may be multiple stable states in the ZBD (other than the commonly reported VAN and HAN states) which are distinguished by their defect locations. The THAN state has not been reported experimentally to our knowledge. We suggest two potential reasons for this: (i) the THAN state may be a "shallow" energy minimum that is easily destabilized by mechanical or field-related effects and (ii) the THAN state is an intermediate state between the VAN and HAN states and may be optically similar to the VAN and HAN states, within experimental resolution. Secondly, we recover the

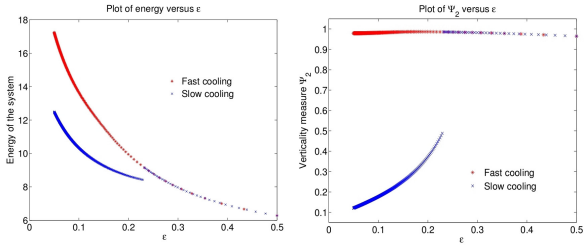

Fig. 6: Switching via temperature: Energy branches for $\epsilon \in (0.05, 0.5)$ with HAN (lower) and THAN (upper) states (left) and vertical measure Ψ_2 plotted against ϵ (right). Further simulations suggest that, once the system reaches $\epsilon = 0.05$, the current state is trapped even for values $\epsilon < 0.05$.

OR phenomenon around the defects in the THAN and HAN states and the biaxial rings extend as stable biaxial cylinders (with an annular cross-section) into the ZBD interior, along the entire ZBD length. There are examples of symmetry-breaking solutions in LCs, e.g. the OR phenomenon in a spherical droplet breaks the spherical symmetry of the so-called radial-hedgehog solution [13]. Therefore, it is interesting to find stable translationally invariant solutions in the 3D ZBD with macroscopic biaxial cylinders and one could exploit such cylinders for new applications. Recent work shows that "biaxial" dynamics can have a strong electro-optic signature, amenable to experimental tests [3, 4]. For example, the HAN-to-VAN switching will involve annihilation of the biaxial rings and this annihilation could be accompanied by a strong electro-optic signal. Finally, we demonstrate temperature-mediated dynamics in 2D and 3D, with no electric fields. Switching processes in LC-based devices are typically induced by electric fields [6,11,17]. Our work suggests that critical voltages may strongly depend on temperature and devices may have an "optimal operating temperature" corresponding to minimum critical voltages. Finally, we expect that (strong) biaxiality is a localized phenomenon near interfaces or defects for micron-scale devices. Recent work shows that one might obtain global biaxial OR patterns in sub micron-scale devices [15]. In such cases, it would be interesting to carry out two parallel studies: uniaxial simulations with $\beta^2 = 0$ (biaxiality "turned off") and full biaxial simulations, followed by a comparison between the uniaxial and biaxial predictions. This will be pursued in future work.

* * *

The authors thank the referees for useful comments and suggestions which much improved the manuscript. The authors thank Patrick Schreier for his MATLAB finite element package and his help during implementation. We thank Peter Howell, Victor Burlakov and Nigel Mottram for fruitful discussions. AM is supported by an EPSRC Career Acceleration Fellowship, EP/J001686/1, an OCCAM Visiting Fellowship and a Keble Research Grant. AR is supported by KAUST, Award No. KUK-C1-013-04 and the John Fell OUP fund.

REFERENCES

[1] de Gennes P.-G. and Prost J., *The Physics of Liquid Crystals (International Series of Monographs on Physics)* 2nd Edition (Oxford University Press, USA) 1995.
[2] Dunmur D., and Sluckin T. J., *Soap, Science, and Flat-Screen TVs: A History of Liquid Crystals* (OUP Oxford) 2010.
[3] Amoddeo A., Barberi R. and Lombardo G., *Phys. Rev. E*, **85** (2012) 061705.
[4] Ambrozic M., Bisi F. and Virga E., *Continuum Mechanics and Thermodynamics*, **20** (2008) 193.
[5] Mottram N. and Newton C., *Research Report: Introduction to Q-tensor theory*, **10** (2004) .
[6] L.A.Parry-Jones and S.J.Elston, *Journal of Applied Physics*, **97** (2005) .
[7] Jones J. C., *SID Symposium Digest of Technical Papers*, **38** (2007) 1347.
[8] *Homepage of zbd.solutions* (2013). `http://www.zbdsolutions.com/`
[9] Brown C. V., Towler M. J., Hui V. C. and Bryan-Brown G. P., *Liquid Crystals*, **27** (2001) 233.
[10] Ladak S., Davidson A., Brown C. V. and Mottram N. J., *Journal of Physics D: Applied Physics*, **42** (2009) 085114.
[11] Parry-Jones L. A., Meyer R. B. and Elston S. J., *Journal of Applied Physics*, **106, 014510** (2009) .
[12] Kralj S., Rosso R. and Virga E., *Phys. Rev. E*, **81** (2010) 021702.
[13] Schopohl N. and Sluckin T. J., *Phys. Rev. Lett.*, **59** (1987) 2582.
[14] Kralj S. and Virga E. G., *J. Phys. A: Math. Gen.*, **34** (2001) 829.
[15] Kralj S. and Majumdar A., *Under review in Proceedings of Royal Society*, (2013) .
[16] Andrienko D. and Allen M. P., *Phys. Rev. E*, **61** (2000) 504.
[17] T.J.Spencer, J.C.Jones, R.M.Amos and C.M.Care, *Physical Review E*, **82** (2010) 021702.
[18] Willman E. J., *http://www.ee.ucl.ac.uk/ ewillman/EJWthesis.pdf* 2009.
[19] Majumdar A., *European J. Appl. Math.*, **21** (2010) 181.
[20] Luo C., Majumdar A. and Erban R., *Phys. Rev. E*, **85** (2012) .
[21] Tasinkevych M., Silvestre N. M. and da Gama M. M. T., *New Journal of Physics*, **14** (2012) 073030.
[22] Bartels S., *J. Comput. Math.*, **27** (2009) 170.
[23] Barberi R., Ciuchi F., Durand G., Iovane M., Sikharulidze D., Sonnet A. and Virga E., *The European Physical Journal E*, **13** (2004) 61.
[24] Lombardo G., Ayeb H. and Barberi R., *Phys. Rev. E*, **77** (2008) 051708.
[25] Harnau L. and Dietrich S., *EPL (Europhysics Letters)*, **73** (2006) 28.
[26] Yi Y., Lombardo G., Ashby N., Barberi R., Maclennan J. E. and Clark N. A., *Phys. Rev. E*, **79** (2009) 041701.